Division of labor during biofilm matrix production

Anna Dragoš[1,2,7], Heiko Kiesewalter[1,8], Marivic Martin[1,2,9], Chih-Yu Hsu[3], Raimo Hartmann[4], Tobias Wechsler[5], Carsten Eriksen[6], Susanne Brix[6], Knut Drescher[4,7,10], Nicola Stanley-Wall[3,11], Rolf Kümmerli[5,12], Ákos T. Kovács[1,2,#,13]

[1] Bacterial Interactions and Evolution Group, Department of Biotechnology and Biomedicine, Technical University of Denmark, Kgs Lyngby, 2800, Denmark

[2] Terrestrial Biofilms Group, Institute of Microbiology, Friedrich Schiller University Jena, Jena, 07743, Germany

[3] School of Life Sciences, University of Dundee, Dundee, DD1 5EH, United Kingdom

[4] Max Planck Institute for Terrestrial Microbiology, Marburg, 35043, Germany

[5] Department of Plant and Microbial Biology, University of Zürich, Zürich, 8057, Switzerland

[6] Disease Systems Immunology Group, Department of Biotechnology and Biomedicine, Technical University of Denmark, Kgs Lyngby, 2800, Denmark

[7] Department of Physics, Philipps University, Marburg, 35037, Germany

Correspondence: atkovacs@dtu.dk

[#] Lead contact

[7] Twitter: @Anna_Dragos

[8] Twitter: @h_kiesewalter

[9] Twitter: @MartinMavs

[10]Twitter: @knutdrescher

[11] Twitter: @Bacteriacities

[12] Twitter: @RolfsMicrobes

[13] Twitter: @EvolvedBiofilm

Summary

Organisms as simple as bacteria can engage in complex collective actions, such as group motility and fruiting body formation. Some of these actions involve a division of labor, where phenotypically specialized clonal subpopulations, or genetically distinct lineages cooperate with each other by performing complementary tasks. Here, we combine experimental and computational approaches to investigate potential benefits arising from division of labor during biofilm matrix production. We show that both phenotypic and genetic strategies for a division of labor can promote collective biofilm formation in the soil bacterium *Bacillus subtilis*. In this species, biofilm matrix consists of two major components; EPS and TasA. We observed that clonal groups of *B. subtilis* phenotypically segregate

into three subpopulations composed of matrix non-producers, EPS-producers, and generalists, which produce both EPS and TasA. This incomplete phenotypic specialization was outperformed by a genetic division of labor, where two mutants, engineered as specialists, complemented each other by exchanging EPS and TasA. The relative fitness of the two mutants displayed a negative frequency dependence both *in vitro* and on plant roots, with strain frequency reaching a stable equilibrium at 30% TasA-producers, corresponding exactly to the population composition where group productivity is maximized. Using individual-based modelling, we show that asymmetries in strain ratio can arise due to differences in the relative benefits that matrix compounds generate for the collective; and that genetic division of labor can be favored when it breaks metabolic constraints associated with the simultaneous production of two matrix components.

Key words: division of labor, biofilm, *Bacillus subtilis,* phenotypic heterogeneity, cooperation, competition, EPS, TasA

Highlights:

- matrix components EPS and TasA are costly public goods in *B. subtilis* biofilms
- genetic division of labor using Δ*eps* and Δ*tasA* fosters maximal biofilm productivity
- Δ*eps* and Δ*tasA* cooperation is evolutionary stable in laboratory and ecological systems
- costly metabolic coupling of public goods favors genetic division of labor

Introduction

Microbes can act collectively in groups, and thereby substantially influence their local environment to their own benefit. Such beneficial collective actions include the secretion of nutrient-degrading enzymes [1], iron-scavenging siderophores [2], biosurfactants for group motility [3], and structural components for biofilm formation [4,5]. In certain cases, cooperation even involves a division of labor, where subpopulations of cells specialize to perform different tasks [6,7]. Division of labor requires three basic conditions: individuals must exhibit different phenotypes (task allocation), the interaction between phenotypes must be cooperative, and all individuals must gain an inclusive fitness benefit from the interaction [8]. The allocation of tasks can be achieved either at the phenotypic or at the genotypic level. In the phenotypic specialization scenario, each individual carries genetic machineries

for all tasks, but differences in gene expression result in tasks allocation [9]. In the genotypic specialization scenario, individuals carry only the genetic machinery for their own specialist task [9].

Both types of division of labor have been proposed to occur in microbes. For instance, during sliding colony expansion *Bacillus subtilis* cells phenotypically differentiate into surfactant producers and matrix producers where the role of the first is to reduce surface tension, while the latter allows expanding colony 'arms' to form and explore new territories [7]. Given the high relatedness between cells, specialization is likely beneficial for the group as a whole [8], with individuals gaining an inclusive fitness benefit from helping their clone mates [10–12]. However, division of labor has recently also been documented between genetically different strains or species [13,14].Cooperative division of labor based on genetic differentiation seems to evolve both frequently and reproducibly [14,15], lending support for the so-called Black Queen hypothesis, which depicts the microbial world as a network of interdependencies between species [16].

While our understanding of division of labor in microbes deepens [7,13,14], it has remained unclear what the advantages and disadvantages of the phenotypically vs genetically determined division of labor are, and which form yields higher fitness returns for the specialists and the community as a whole. When considering division of labor based on the exchange of two beneficial public goods, a phenotypic specialization could offer advantages because cells producing the two public goods will naturally be close to one another due to binary cell division. Close spatial proximity is essential for efficient public good sharing [18], yet might be compromised with genetically determined division of labor, as spatial separation of partners can readily occur and the switching of specialization states is not possible [19]. Conversely, genetically determined division of labor might offer advantages because it allows a complete decoupling of traits at the metabolic level. Specifically, the expression of two alternative synthetic pathways (both bearing a metabolic burden) can be terminally allocated into two different genetic lineages [20]. Finally, it has been argued that in contrast to phenotypic differentiation, terminal genetic divergence bears risks of conflicts such as social exploitation because relatedness between interacting partners is reduced; potentially leading to diverging interests between partners [19].

Here, we focus on identifying the costs and benefits associated with different division of labor strategies for biofilm formation in the common soil and plant-colonizing bacterium *B. subtilis*, in terms of individual and collective productivity. Biofilms represent the most common lifestyle of bacteria, where cells are in close proximity to one another, embedded in extracellular matrix (ECM) [21]. There

is ample opportunity for division of labor over matrix construction, because ECM usually consists of multiple secreted compounds that form a mesh of complex exopolysaccharides (EPS) and structural proteins, sometimes accompanied by extracellular DNA (eDNA). While the presence of eDNA can be the consequence of cell death [22], the production of matrix exopolysaccharides and proteins tends to be triggered by cooperative signaling [23], cues released by competitors [24], or specific nutrient components [25,26]. As the synthesis of large polymers is metabolically costly, tight regulation of matrix gene expression is often in place, and it has been suggested that the overall metabolic costs for the community may be reduced by assigning matrix production only to a subpopulation of cells [27]. Here we propose an alternative scenario involving division of labor, where subgroups of individuals within a biofilm each specialize (either phenotypically or genetically) in the production of a different matrix component, which are then shared at the level of the group.

Our model system involves *B. subtilis* forming robust, wrinkly pellicle biofilms that reside at the oxygen rich liquid-air interface [28]. Increasing cell density of the planktonic cells results in a decreasing oxygen concentration in the bottom layers of the static medium. Aerotaxis of *B. subtilis* leads to an accumulation of cells near the liquid-air interface and eventually a colonization of the surface in a form of a densely packed pellicle biofilm. During pellicle development transcription of the matrix-related operons *epsA-O* and *tapA-sipW-tasA* is derepressed [27,29–31] eventually allowing synthesis of the biofilm exopolysaccharide (EPS), and the structural protein TasA [32,33]. Mutants lacking either EPS or TasA cannot establish pellicle biofilms individually, but they can complement each other in co-culture, indicating that both matrix components are necessary for pellicle biofilms and that they are shared [32,34,35].

Using a mixture of fitness assays, single-cell gene expression analyses and mathematical modelling, we show that the two matrix components EPS and TasA are indeed costly to produce. We further found that cells within a biofilm phenotypically differentiate into three distinct subpopulations consisting of cells producing either both of the matrix components, EPS alone, or none of the two components. We then demonstrate that in terms of group productivity, genetic division of labor for matrix construction can be superior to the phenotypic differentiation strategy present in the wild type. Specifically, biofilm productivity was maximized at an intermediate mixing ratio of mutants deficient for either EPS or TasA, both in pellicle biofilms grown in the laboratory, and in biofilms grown on plant hosts. Crucially, the Δ*eps* : Δ*tasA* proportion at which biofilm productivity maximization occurred, represents a stable equilibrium.

143 **RESULTS**

144

145 **The matrix components EPS and TasA serve as costly public goods**

146 Components of bacterial extracellular matrix are often large, complex polymers, which can potentially
147 bear significant metabolic production costs [1,36]. To demonstrate the costs associated with the
148 production of EPS and TasA in our *B. subtilis* strain (NCBI 3610), we competed the non-producing
149 mutants Δ*eps* and Δ*tasA* against the wild type (WT) under conditions where matrix is synthesized but
150 not required for survival [37], which is up to 16 hours of growth, prior to surface colonization (Movie
151 S1; see Methods). We confirmed that in the pre-pellicle phase the WT, Δ*eps*, and Δ*tasA* strains first
152 grow exponentially before reaching the early stationary phase (Figure S1A). While strains expressed
153 the corresponding matrix components (Figure S1B-D assays based on fluorescent transcriptional
154 reporters P_{eps}-*gfp* and P_{tapA}-*gfp*), the expression patterns slightly varied between the WT and the
155 mutants. The expression of P_{tapA} in Δ*eps* and P_{eps} in Δ*tasA* were slightly stronger and weaker,
156 respectively, with shift towards more homogenous expression in both mutants (Figure S1C). Under
157 these conditions, our growth competition fitness assay revealed significant costs for both matrix
158 components (Figure 1A). The fact that Δ*eps* had significantly higher relative fitness than Δ*tasA* in
159 pairwise competition against the WT suggests that EPS synthesis bears a higher cost than TasA
160 production under these conditions (Figure 1A).

161

162 Next, we examined sharing of the two components. We began with complementation assays mixing
163 the two mutants (Δ*eps* and Δ*tasA* single deletion mutants) in 1:1 ratios. In line with previous reports
164 [32,34,35], we found that the mutants could not establish pellicles when grown in monocultures, but
165 complemented each other when co-cultured, indicating that EPS and TasA can be shared (Figure 1B,C).
166 Since TasA was previously depicted as a cell-associated amyloid fiber, anchored through the accessory
167 protein TapA to the cell [34], we performed additional experiments to confirm cross-
168 complementation. Specifically, we added conditioned media from the EPS and TasA producers to
169 growing cultures of the Δ*eps* and Δ*tasA*, respectively, and quantified their surface colonization ability.
170 We observed that the conditioned medium from the WT or the complementary mutant significantly
171 improved pellicle formation as compared to the control, with the effect being more pronounced for
172 the Δ*eps* than the Δ*tasA* mutant (Figure 1D). This result suggests that the spent medium obtained from
173 the WT and Δ*tasA* contained freely released EPS which could complement the Δ*eps* strain. Similarly,
174 WT and Δ*eps* released a portion of TasA into the medium, that could partially complement the Δ*tasA*
175 phenotype.

176

177 As the above results (Figure 1D) suggest that the matrix components EPS and TasA differ in the extent
178 to which they are shared, pointing towards stronger privatization of TasA, we hypothesized that
179 efficient mixing of EPS-producers and TasA-producers is necessary for successful complementation.
180 To test the role of mixing we took advantage of a previously observed motility effect on cell
181 assortment in pellicle biofilms [38]: Cells lacking a functional flagellum (Δ*hag*) are less efficient in
182 swimming to the top of the liquid, which likely results in very low number of founder cells carrying the
183 Δ*hag* mutation (compared to WT) in the pellicle. As a result, pellicles formed by two isogenic Δ*hag*
184 strains labeled with different fluorophores, contain large clusters of cells of the same lineage,
185 indicating limited genotype mixing [38]. As expected, the efficiency of complementation between EPS-
186 and TasA-producers was negatively affected in the Δ*hag* genetic background as compared to the
187 control with functional flagella (Figure S2A). Finally, the spatial assortment of cells in the pellicles
188 formed by mixtures of Δ*eps* and Δ*tasA* and pellicles formed by the WT were compared using a density
189 correlation function quantification method (see Methods), to assess the spatial effects of genetic
190 division of labor (Figure S2B-D). The level of spatial strain mixing was slightly higher in pellicles formed
191 by mixtures of Δ*eps* and Δ*tasA* (regardless of the fluorescence reporter combination) as compared to
192 pellicles formed by the WT (Figure S2C,D).
193
194 Altogether, these results confirm that both matrix components EPS and TasA can be shared and that
195 robust pellicle biofilm formation depends on the efficient exchange of these compounds.
196
197 **Wild type cells exhibit phenotypic heterogeneity in the expression of matrix components**
198 As EPS and TasA are costly to produce (Figure 1A) and can both be shared between the producers and
199 non-producers (Figure 1B-D), we hypothesized that phenotypic differentiation into EPS-producers and
200 TasA-producers could occur and form the basis of a division of labor in WT *B. subtilis* populations
201 during pellicle formation. To test for phenotypic heterogeneity of *eps* and *tasA* expression at the single
202 cell level, we used a reporter strain carrying a promoter fusion of the *eps* promoter to *gfp* (P_{eps}-*gfp*)
203 and an analogous reporter for the *tapA* promoter based on *mKate* (P_{tapA}-*mKate*) at two distinct
204 genomic loci (see Methods, Table S1). As a control, we used the P_{tapA}-*gfp* P_{tapA}-*mKate* strain (see
205 Methods, Table S1) for which no phenotypic heterogeneity and a linear correlation between the two
206 fluorescence channels was expected. Fluorescent images of mature pellicles of the WT P_{eps}-*gfp* P_{tapA}-
207 *mKate* strain and the control WT P_{tapA}-*gfp* P_{tapA}-*mKate* strain were captured using confocal laser
208 scanning microscopy (CLSM). While the control strain showed a clear spatial correlation between GFP
209 and mKate fluorescence intensities, this was not the case for the WT P_{eps}-*gfp* P_{tapA}-*mKate* strain (Figure
210 2A). Specifically, large bright clusters of strong GFP signal could be observed in locations in which there
211 was reduced mKate fluorescence, suggesting the presence of a subpopulation that is partially

212 specialized for EPS production (Figure 2A). We further performed quantitative analyses of the
213 fluorescent images by artificially dissecting the images into small cubes and quantifying the GFP- and
214 mKate-signal intensities in each cube (see STAR Methods). This allowed us to examine whether GFP
215 and mKate fluorescence intensities linearly correlate in space. Such linear correlation was expected
216 from the control strain (WT P_{tapA}-*gfp* P_{tapA}-*mKate*) and could be the case for the P_{eps}-*gfp* P_{tapA}-*mKate*
217 strain if *eps* and *tasA* were expressed by the same population of cells. The analysis confirmed that for
218 biofilms made by the P_{tapA}-*gfp* P_{tapA}-*mKate* strain, signal intensities from GFP and mKate channels
219 showed strong linear correlation in space, this correlation was much weaker in case of the P_{eps}-*gfp*
220 P_{tapA}-*mKate* strain (Figure 2B, Figure S3A).
221
222 The above experiment suggests that matrix-expressing subpopulations of WT *B. subtilis* exhibit a
223 certain degree of phenotypic differentiation into cells that produce mostly EPS and cells that produce
224 both EPS and TasA (generalists). To confirm this pattern, we analyzed single cells extracted from
225 pellicles using fluorescence-guided flow cytometry (FC). FC analyses were performed at 3 time points
226 during pellicle development (24, 48 and 72 hours) and included controls with strains carrying single
227 reporter fusions (see Methods, Table S1). These analyses revealed the presence of 3 distinct
228 subpopulations of cells: (i) matrix-OFF cells where fluorescence signals from both the P_{eps} and P_{tapA}
229 promoters were below the detection thresholds; (ii) matrix-ON cells where there was a positive linear
230 correlation of the signals from the P_{eps} and P_{tapA} promoters: (iii) EPS-ON cells, containing a fluorescent
231 signal from P_{eps}, but not from P_{tapA} (Figure 2C, Figure S3B). Differences in relative frequencies of P_{eps}-
232 *gfp* and P_{tapA}-*mKate* ON cells were not due to the use of different fluorescent reporters, as evidenced
233 by our FC control experiments where strains carrying either a P_{tapA}-*gfp* or a P_{tapA}-*mKate* reporter
234 construct showed identical frequencies of ON cells (Figure S3C,D). Thus, our FC experiments confirmed
235 that the expression of the two major matrix promoters P_{eps} and P_{tapA} is not perfectly correlated, which
236 likely translates into phenotypic diversity at the level of EPS and TasA production in wild type *B. subtilis*
237 pellicles.
238
239 **Genetic division of labor yields higher biofilm productivity than phenotypic differentiation**
240 Although the above data indicate that wild type cells differentiate into EPS-producers, generalists, and
241 non-producers during pellicle biofilm formation, this pattern does not resemble the canonical
242 principle of division of labor where distinct subpopulations of cells are expected to either commit
243 completely to TasA or EPS production. The incomplete specialization could be due to regulatory
244 constraints. For instance, it is known that the *epsA-O* and *tapA-sipW-tasA* operons share multiple
245 regulators, suggesting that some level of parallel expression (either on or off) at the single cell level is
246 expected [39,40].

247

248 We thus wondered whether an incomplete specialization represents a beneficial strategy or whether
249 it can be outperformed by a genetically determined specialization, where cells are ultimately
250 constrained in the production of either TasA or EPS. To address this question, we studied the division
251 of labor between Δ*tasA* as the exclusive EPS-producer and Δ*eps* as the exclusive TasA producer. In a
252 first experiment, we mixed the exclusive EPS- and TasA-producers at different ratios and examined
253 the productivities of pellicles (Figure 3A). We found that pellicle productivity varied in response to
254 strain frequency, and peaked at a strain ratio of approximately 30 % Δ*eps* : 70% Δ*tasA* (Figure 3A).
255 Interestingly, the group productivity of mixtures close to this optimal ratio was significantly higher
256 than the WT productivity, indicating that the genetic division of labor over matrix construction
257 outperforms the native phenotypic differentiation observed in the WT (Figure 3A).
258

259 **Genetic division of labor is evolutionarily stable in pellicles and on plant roots**

260 We next asked whether such genetic division of labor, which yields the highest fitness returns at a
261 strain ratio of approximately 30:70, represents a stable equilibrium or simply a transient phenomenon.
262 To test this possibility, we competed the Δ*eps* strain against the Δ*tasA* strain across a range of
263 frequencies (1% to 99 %), over the full cycle of pellicle growth (from inoculation until formation of
264 robust, wrinkly pellicle after 48 hours). These competitions revealed that the relative fitness of Δ*eps*
265 followed a negative frequency-dependent pattern: Δ*eps* outcompeted Δ*tasA* when rare, but lost the
266 competition when common (Fig. 3B). Strikingly, the two strains showed equal competitiveness at
267 starting frequencies between 20% - 30% Δ*eps*, thus exactly at the strain ratio where biofilm
268 productivity is maximized. These findings strongly suggest that, regardless of the metabolic cost
269 imbalance between the two matrix components, stable coexistence of the EPS and TasA producers is
270 favored in the pellicle, with strain frequency evolving towards the optimum in terms of biofilm
271 biomass productivity (Figure 1A, Figure 3B).
272

273 To test whether stable genetic division of labor could also manifest in a relevant ecological
274 environment, we repeated several key experiments using plant root associated biofilms. Specifically,
275 we subjected the roots of *Arabidopsis thaliana* seedlings to colonization by the WT, or a mixture of
276 Δ*eps* and Δ*tasA* strains at a 50:50 ratio, or monocultures of the two mutants (see Methods). Each
277 strain carried a constitutive fluorescent reporter to allow biofilm visualization by CLSM (see methods,
278 Table S1). In line with previous studies [41], both the WT and the mixture of Δ*eps* and Δ*tasA* strains
279 were able to produce thick biofilms on the roots, which was not the case for the Δ*eps* and Δ*tasA*
280 mutants grown in monocultures on the plant root (Figure 4A,B). Analogous to the pellicles, we found
281 that the productivity of root biofilms was significantly higher for the Δ*eps* + Δ*tasA* mixture as compared

282 to the WT. Next, we estimated the relative frequencies of Δ*eps* and Δ*tasA* mutants in the mixed biofilm
283 on the root, based on total pixel volumes (see methods), and found that the mutant frequency settled
284 at the optimal ratio of 20% - 30% Δ*eps* (Figure 4B,C). In contrast, the frequency remained close to
285 0.5:0.5 in our control mixtures of two WT strains labeled with different fluorescent reporters (Figure
286 4B,C). Altogether, our experiments demonstrate that the genetically hard-wired division of labor
287 between EPS- and TasA-producers provides fitness benefits not only in pellicles, but also on plant
288 roots.
289
290 **Simulating pellicle formation to understand the drivers of genetic division of labor**
291 To better understand the conditions required for genetic division of labor to evolve between EPS- and
292 TasA-producing specialists, we used an individual-based modelling platform, specifically developed to
293 simulate microbial interactions [42]. The platform consists of a two-dimensional toroidal surface,
294 where bacterial cells are modeled as discs. Bacteria are seeded in low numbers to their *in-silico*
295 habitat, and are then allowed to consume resources, grow, divide, disperse, and produce public goods
296 according to specified parameters for 10,000 time steps (see methods for fitness equations). The
297 system keeps track of both bacterial strains and their public goods over time and space, and closely
298 recovers patterns of real pellicle formation (Figures S4).
299
300 First, we examined the performance of a wildtype (WT) strain, which simultaneously produces two
301 complementary public goods, representing EPS and TasA. Simulations started with eight cells placed
302 in the center of the landscape to mimic the early phase of pellicle formation. Cells grew and divided
303 at a basic rate (μ). Cells additionally produced diffusible public goods at a constant rate. Public goods
304 diffuse randomly, can decay or generate fitness benefits for receiver cells. While each public good
305 generates a benefit on its own, synergistic benefits accrue to cells that encounter the two
306 complementary public goods within a certain time frame. Using this setup, we found that WT biofilm
307 productivity peaked with lower public good diffusion *d* (Figure S5A), indicating that reduced diffusion
308 minimizes the loss and improves sharing of public goods. Since our experimental data suggest that
309 TasA and EPS differ in the level of sharing, and thus in the relative benefit these goods can generate
310 for the group, we varied this parameter in our model, but found that it did not affect the productivity
311 of WT pellicles (Figure S5B). We then implemented metabolic constraints (via the factor *f*, defined in
312 Eq. (1) in the STAR Methods) in the WT to account for the possibility that the simultaneous production
313 of two public goods exceeds the sum of each individual public good ($f > 1$) [20]. We observed that
314 biofilm productivity sharply declined with increased levels of constraints (Figure S5C).
315

316 Next, we considered different levels of phenotypic heterogeneity in the WT by starting simulations
317 with different ratios of specialist and non-specialist cells (Figure S5D-F). We found that any level of
318 phenotypic heterogeneity outperformed uniform trait expression at the beginning of pellicle
319 formation (Figure S5D). Conversely, the most beneficial strategies in more mature pellicles were either
320 complete specialization or no specialization at all (Figure S5E,F). We hypothesize that no specialization
321 performs well because it allows efficient public good sharing at higher cell densities, and complete
322 specialization is beneficial because it breaks metabolic constraints. In contrast, any intermediate form
323 of phenotypic heterogeneity suffers from reduced sharing and sustained metabolic constraints, and
324 should thus be selected against. This finding might explain why the *B. subtilis* WT strain showed
325 relatively low levels of phenotypic heterogeneity.
326
327 We then asked whether two genetically fixed mutants, producing either one or the other public good
328 (i.e. mimicking Δ*eps* and Δ*tasA* mutants) can complement each other. Similar to our empirical
329 observations, we found successful complementation between the two specialist strains, with pellicle
330 productivity peaking at intermediate mixing ratios (Figure 5A). Moreover, the relative fitness of the
331 Δ*eps* strain exhibited negative-frequency dependence (Figure 5B), and the point of fitness equilibrium
332 occurred exactly at the productivity peak of the group. Next, we implemented the experimental
333 observation that TasA yields lower benefits than EPS. We again observed successful complementation,
334 but pellicle productivity reached higher levels and peaks shifted to lower frequencies of the Δ*eps*
335 strain, in the case of a greater benefit imbalance between the two public goods (Figure 5C). The
336 relative fitness of the Δ*eps* strain again followed a negative-frequency dependence with the point of
337 intersection being exactly at the pellicle productivity peak (Figure 5D). To examine whether the
338 reciprocal symmetric exchange of public goods is the reason for why strain equilibrium frequency
339 coincides with maximal group productivity, we simulated a scenario of asymmetrical public good
340 exchange between a strain producing both public goods and a strain producing a single public good
341 (Figure 5E,F). For this scenario, we found that the relationship between strain equilibrium and maximal
342 group productivity breaks: the strain producing only one public good experienced relative fitness
343 advantages at all strain frequencies, driving strain frequency away from maximal group fitness.
344
345 Finally, we asked whether genetic division of labor between the Δ*eps* and Δ*tasA* strains can
346 outperform the WT strategy, as observed in our empirical experiments. However, in the absence of
347 any metabolic constraints (f = 1), the WT pellicle productivity was 1714 ± 39 cells (mean ± SE, with
348 intermediate diffusion d = 5), and thus by far higher than productivity in any of the complementation
349 scenarios (Figure 5). Conversely, when the WT faces metabolic constraints, we found a parameter

350 space ($f > 1.1$), in which pellicle productivity of complementing strains exceeds wildtype performance
351 (Figure 5C).
352
353 Taken together, our simulations recover the key features of our experimental system and suggest that
354 the reciprocal symmetrical exchange of public goods under conditions of relatively low diffusion
355 together with the decoupling of metabolic constraints are the preconditions required for the evolution
356 of stable genetic division of labor over biofilm matrix production.
357
358
359 **DISCUSSION**
360
361 Despite their unicellular simplicity, microbes can coordinate complex behaviors as a group. Some of
362 these multicellular behaviors involve division of labor between phenotypically distinct subpopulations
363 [7,17], or even different genetic lineages [14]. Here we deployed a combination of experiments and
364 simulations to directly compare these two alternative cooperative strategies. By focusing on the
365 production of two biofilm matrix components in *B. subtilis*, we found evidence for significant, yet
366 incomplete phenotypic specialization in matrix production among clonal cells of the wild type strain.
367 However, this strategy of phenotypic specialization was outperformed by genetic division of labor,
368 where strains, engineered as strict specialists, settled on an equilibrium ratio that maximized biofilm
369 productivity. Our individual-based modeling approach captures the experimental system and reveals
370 that metabolic decoupling of two costly traits can be the key to success for genetic specialization.
371
372 While we demonstrate that *B. subtilis* WT displays partial phenotypic differentiation at the level of
373 matrix production, we might ask why this form of specialization is not more pronounced, especially in
374 the context of the reported fitness benefits that can accrue from complete genetic specialization (Fig.
375 3A). One explanation might be that the *epsA-O* and *tapA-sipW-tasA* operons share multiple regulators,
376 such that some level of parallel expression is inevitable [39,40,43,44]. Still, there could be certain
377 mechanisms in place to decouple EPS and TasA production, for example a positive feedback where
378 EPS prevents autophosphorylation of the EpsAB kinase, allowing activation of the EpsE glycosyl-
379 transferase, thereby promoting EPS-synthesis [45]. It was also proposed that the major matrix
380 repressor SinR, acts differently on P_{eps} and P_{tapA} promoters. Specifically, in the case of P_{eps} it directly
381 competes with an activator RemA for the binding site upstream of the promoter, thereby serving as
382 an anti-activator, while in case of P_{tapA} it binds simultaneously with RemA, probably serving as a
383 repressor [44]. The opposing relationship between SinR and RemA may lead to an outburst of *epsA-O*
384 expression in a subpopulation of cells, while *tapA-sipW-tasA* remains under tighter control of SinR.

385 While these regulatory mechanisms could allow for some heterogeneity in gene expression, complete
386 specialization seems impossible. Another possibility is that such complete specialization with 30:70
387 frequencies of TasA-producers and EPS-producers, does not always reflect an optimal solution. Biofilm
388 formation is only one out of multiple cooperative survival strategies of *B. subtilis* and each strategy
389 might require different optimal ratios of generalists and specialists. For instance, the presence of
390 generalists that can produce both EPS and TasA may be favored during social spreading on solid
391 surfaces, where both components are important [7], but where the diffusion of these public goods is
392 reduced compared with pellicle growth conditions.
393
394 Our findings on successful genetic division of labor between specialized strains, producing either EPS
395 or TasA, show that strain frequency settles as a stable frequency of approximately 70:30. Our model
396 suggests that the dominance of EPS-producers in biofilms may be driven by a higher relative benefit
397 of EPS compared with TasA. In addition, the altered matrix gene expression patterns in Δ*eps*
398 (overproducing TasA) and Δ*tasA* (reduced EPS production) suggest that a higher proportion of Δ*tasA*
399 might be required for stable pellicle production. Perhaps the two matrix components engage in an
400 interaction that alters their biochemical properties. One possibility is that upon interaction with EPS,
401 TasA becomes less soluble and vice versa. This could explain a decreased complementation efficiency
402 of Δ*eps* and Δ*tasA* strains by the spent media obtained from the WT (Figure 1D). Recent work suggests
403 that the structural functionality of TasA fibers may directly depend on the presence of EPS in the
404 extracellular environment [46].
405
406 The 70:30 population structure is stable in typical laboratory setup (pellicle biofilms) and in plant root-
407 associated biofilms. Although the genetic division of labor arose as the winning strategy, our study
408 also points towards the canonical problem associated with fixed cooperation strategies: limited mixing
409 of strains prevents efficient genetic division of labor [19]. Specifically, we found that the
410 complementation between EPS- and TasA-producers was ineffective in experiments with flagellum-
411 deficient strains, which exhibit a decreased level of mixing, thereby reducing public good sharing and
412 the formation of robust pellicle biofilms. Mathematical models ([47], our model) suggest that
413 complementation is most efficient when strain mixing is high, but the diffusion of public goods is
414 reduced, conditions that foster efficient public good exchange between neighbors and prevent losses
415 due to diffusion. A further complication is that the goods to be exchanged might often vary in their
416 diffusion properties. Our assays, for instance, suggest that the diffusion and sharing of TasA is rather
417 limited compared to EPS. We argue that such low diffusion rates must be compensated by an
418 increased spatial mixing of the cooperation partners. Therefore, in opposition to "xenophobic"

419 mechanisms employed by microbes to avoid strangers [48–50], "xenophilic" strategies might be
420 crucial for genetic division of labor.
421
422 In conclusion, our study offers major insights into the evolution of division of labor. First, it shows that
423 genetic specialization can be superior over phenotypic division of labor because it enables to break
424 metabolic and regulatory constraints prevailing in organisms that remain totipotent. Second,
425 sophisticated genetic division of labor can occur in simple organisms such as bacteria. Finally, genetic
426 division of labor, based on the reciprocal exchange of public goods, could represent an evolutionary
427 stable strategy, with strain frequency evolving towards an equilibrium that maximizes group
428 productivity. Important to consider is whether de novo mutations may occur in the long term and
429 disturb the observed equilibrium. For instance, a double mutant Δ*eps*Δ*tasA*, which is deficient in both
430 matrix components could exploit the complementing partners and derail the genetic division of labor.
431 Future studies will need to experimentally test whether the reported cases of genetic division of labor
432 are evolutionary stable in the long run.
433
434
435 **Author Contributions**
436 A.D. and Á.T.K. conceived the project, A.D., H.K., M.M., C.-Y.H., and C.E. performed experiments, R.H.
437 and K.D. analyzed quantitatively the CLSM imaging data, C.-Y.H., N.S.-W., C.E. and S.B. analyzed the
438 flow cytometry results, T.W. and R.K. performed modeling and analyzed the simulations. A.D., R.K.,
439 and Á.T.K. wrote and corrected the manuscript. All authors contributed critically to the drafts and gave
440 final approval for publication.
441
442 **Acknowledgement**
443 This work was funded by the Deutsche Forschungsgemeinschaft (DFG) to Á.T.K. (KO4741/2.1) within
444 the Priority Program SPP1617. A.D. was supported by a fellowship from Alexander von Humboldt
445 foundation. R.K. was funded by the Swiss National Science Foundation (grant no. PP00P3_165835) and
446 the European Research Council (ERC-CoG no. 681295). This work was further supported by BBSRC
447 grant code BB/P0001335 to N.S.-W., a scholarship from BeautyHsiao Biotech. Inc to C-Y.H., the
448 European Research Council (ERC-StG no. 716734) and the Human Frontier Science Program
449 (CDA00084/2015-C) to K.D., and a Start-up grant from the Technical University of Denmark to Á.T.K.
450 Work in the laboratory of Á.T.K. is partly supported by the Danish National Research Foundation
451 (DNRF137) for the Center for Microbial Secondary Metabolites. We acknowledge the help of Dr.
452 Rosemary Clarke for assistance with flow cytometry performed at the University of Dundee.

453

454 **REFERENCES**

455

456 1. Drescher, K., Nadell, C.D., Stone, H.A., Wingreen, N.S., and Bassler, B.L. (2014). Solutions to
457 the public goods dilemma in bacterial biofilms. Curr. Biol. *24*, 50–55.
458 2. Harrison, F., and Buckling, A. (2009). Siderophore production and biofilm formation as linked
459 social traits. ISME J. *3*, 632–634.
460 3. Pollak, S., Omer-Bendori, S., Even-Tov, E., Lipsman, V., Bareia, T., Ben-Zion, I., and Eldar, A.
461 (2016). Facultative cheating supports the coexistence of diverse quorum-sensing alleles. Proc.
462 Natl. Acad. Sci. U. S. A. *113*, 2152–7.
463 4. Boyle, K.E., Heilmann, S., van Ditmarsch, D., and Xavier, J.B. (2013). Exploiting social evolution
464 in biofilms. Curr. Opin. Microbiol. *16*, 207–12.
465 5. Dragoš, A., and Kovács, Á.T. (2017). The peculiar functions of the bacterial extracellular
466 matrix. Trends Microbiol. *25*, 257–266.
467 6. Strassmann, J.E., and Queller, D.C. (2011). Evolution of cooperation and control of cheating in
468 a social microbe. Proc. Natl. Acad. Sci. U. S. A. *108*, 10855–62.
469 7. van Gestel, J., Vlamakis, H., and Kolter, R. (2015). From cell differentiation to cell collectives:
470 *Bacillus subtilis* uses division of labor to migrate. PLoS Biol. *13*, e1002141.
471 8. West, S.A., and Cooper, G.A. (2016). Division of labour in microorganisms: an evolutionary
472 perspective. Nat. Rev. Microbiol. *14*, 716–723.
473 9. Wahl, L.M. (2002). The Division of Labor: Genotypic versus phenotypic specialization. Am.
474 Nat. *160*, 135–145.
475 10. Hamilton, W.D. (1964). The genetical evolution of social behaviour. I. J. Theor. Biol. *7*, 1–16.
476 11. Ackerman, J.M., and Kenrick, D.T. (2008). The costs of benefits: Help-refusals highlight key
477 trade-offs of social life. Personal. Soc. Psychol. Rev. *12*, 118–140.
478 12. Refardt, D., Bergmiller, T., and Kümmerli, R. (2013). Altruism can evolve when relatedness is
479 low: evidence from bacteria committing suicide upon phage infection. Proceedings. Biol. Sci.
480 *280*, 20123035.
481 13. D'Souza, G., and Kost, C. (2016). Experimental evolution of metabolic dependency in bacteria.
482 PLoS Genet. *12*, e1006364.
483 14. Kim, W., Levy, S.B., and Foster, K.R. (2016). Rapid radiation in bacteria leads to a division of
484 labour. Nat. Commun. *7*, 10508.
485 15. Germerodt, S., Bohl, K., Lück, A., Pande, S., Schröter, A., Kaleta, C., Schuster, S., and Kost, C.
486 (2016). Pervasive selection for cooperative cross-feeding in bacterial communities. PLOS

487 Comput. Biol. *12*, e1004986.
488 16. Morris, J.J., Lenski, R.E., and Zinser, E.R. (2012). The Black Queen Hypothesis: evolution of
489 dependencies through adaptive gene loss. MBio *3*, e00036-12.
490 17. Mohri, K., Kiyota, Y., Kuwayama, H., and Urushihara, H. (2013). Temporal and non-permanent
491 division of labor during sorocarp formation in the social amoeba *Acytostelium subglobosum* .
492 Dev. Biol. *375*, 202–209.
493 18. Weigert, M., and Kümmerli, R. (2017). The physical boundaries of public goods cooperation
494 between surface-attached bacterial cells. bioRxiv, 119032.
495 19. Oliveira, N.M., Niehus, R., and Foster, K.R. (2014). Evolutionary limits to cooperation in
496 microbial communities. Proc. Natl. Acad. Sci. U. S. A. *111*, 17941–6.
497 20. Rueffler, C., Hermisson, J., and Wagner, G.P. (2012). Evolution of functional specialization and
498 division of labor. Proc. Natl. Acad. Sci. *109*, E326–E335.
499 21. Nadell, C.D., Xavier, J.B., and Foster, K.R. (2009). The sociobiology of biofilms. FEMS
500 Microbiol. Rev. *33*, 206–24.
501 22. Jakubovics, N.S., Shields, R.C., Rajarajan, N., and Burgess, J.G. (2013). Life after death: the
502 critical role of extracellular DNA in microbial biofilms. Lett. Appl. Microbiol. *57*, 467–475.
503 23. Waters, C.M., Lu, W., Rabinowitz, J.D., and Bassler, B.L. (2008). Quorum sensing controls
504 biofilm formation in *Vibrio cholerae* through modulation of cyclic di-GMP levels and
505 repression of *vpsT*. J. Bacteriol. *190*, 2527–36.
506 24. Oliveira, N.M., Martinez-Garcia, E., Xavier, J., Durham, W.M., Kolter, R., Kim, W., and Foster,
507 K.R. (2015). Biofilm formation as a response to ecological competition. PLOS Biol. *13*,
508 e1002191.
509 25. Shemesh, M., and Chai, Y. (2013). A combination of glycerol and manganese promotes biofilm
510 formation in *Bacillus subtilis* via histidine kinase KinD signaling. J. Bacteriol. *195*, 2747–2754.
511 26. Marsden, A.E., Grudzinski, K., Ondrey, J.M., DeLoney-Marino, C.R., and Visick, K.L. (2017).
512 Impact of salt and nutrient content on biofilm formation by *Vibrio fischeri*. PLoS One *12*,
513 e0169521.
514 27. Chai, Y., Chu, F., Kolter, R., and Losick, R. (2007). Bistability and biofilm formation in *Bacillus*
515 *subtilis*. Mol. Microbiol. *67*, 254–263.
516 28. Branda, S.S., Gonzalez-Pastor, J.E., Ben-Yehuda, S., Losick, R., and Kolter, R. (2001). Fruiting
517 body formation by *Bacillus subtilis*. Proc. Natl. Acad. Sci. U. S. A. *98*, 11621–11626.
518 29. Kobayashi, K. (2008). SlrR/SlrA controls the initiation of biofilm formation in *Bacillus subtilis*.
519 Mol. Microbiol. *69*, 1399–1410.
520 30. Cozy, L.M., Phillips, A.M., Calvo, R.A., Bate, A.R., Hsueh, Y.-H., Bonneau, R., Eichenberger, P.,

521 and Kearns, D.B. (2012). SlrA/SinR/SlrR inhibits motility gene expression upstream of a
522 hypersensitive and hysteretic switch at the level of σ^D in *Bacillus subtilis*. Mol. Microbiol. *83*,
523 1210–1228.
524 31. Kearns, D.B. (2013). You get what you select for: better swarming through more flagella.
525 Trends Microbiol. *21*, 508–509.
526 32. Branda, S.S., Chu, F., Kearns, D.B., Losick, R., and Kolter, R. (2006). A major protein
527 component of the *Bacillus subtilis* biofilm matrix. Mol. Microbiol. *59*, 1229–1238.
528 33. Romero, D., Vlamakis, H., Losick, R., and Kolter, R. (2011). An accessory protein required for
529 anchoring and assembly of amyloid fibres in *B. subtilis* biofilms. Mol. Microbiol. *80*, 1155–
530 1168.
531 34. Romero, D., Aguilar, C., Losick, R., and Kolter, R. (2010). Amyloid fibers provide structural
532 integrity to *Bacillus subtilis* biofilms. Proc. Natl. Acad. Sci. U. S. A. *107*, 2230–2234.
533 35. Martin, M., Dragoš, A., Hölscher, T., Maróti, G., Bálint, B., Westermann, M., and Kovács, Á.T.
534 (2017). *De novo* evolved interference competition promotes the spread of biofilm defectors.
535 Nat. Commun. *8*, 15127.
536 36. van Gestel, J., Weissing, F.J., Kuipers, O.P., and Kovács, Á.T. (2014). Density of founder cells
537 affects spatial pattern formation and cooperation in *Bacillus subtilis* biofilms. ISME J. *8*, 2069–
538 79.
539 37. West, S. a, Griffin, A.S., Gardner, A., and Diggle, S.P. (2006). Social evolution theory for
540 microorganisms. Nat. Rev. Microbiol. *4*, 597–607.
541 38. Hölscher, T., Bartels, B., Lin, Y.C., Gallegos-Monterrosa, R., Price-Whelan, A., Kolter, R.,
542 Dietrich, L.E., and Kovács, Á.T. (2015). Motility, chemotaxis and aerotaxis contribute to
543 competitiveness during bacterial pellicle biofilm development. J. Mol. Biol. *427*, 3695–3708.
544 39. López, D., Vlamakis, H., and Kolter, R. (2009). Generation of multiple cell types in *Bacillus*
545 *subtilis*. FEMS Microbiol. Rev. *33*, 152–63.
546 40. Diethmaier, C., Pietack, N., Gunka, K., Wrede, C., Lehnik-Habrink, M., Herzberg, C., Hubner, S.,
547 and Stulke, J. (2011). A novel factor controlling bistability in *Bacillus subtilis* : the YmdB
548 protein affects flagellin expression and biofilm formation. J. Bacteriol. *193*, 5997–6007.
549 41. Beauregard, P.B., Chai, Y., Vlamakis, H., Losick, R., and Kolter, R. (2013). *Bacillus subtilis*
550 biofilm induction by plant polysaccharides. Proc. Natl. Acad. Sci. *110*, 1621–1630.
551 42. Dobay, A., Bagheri, H.C., Messina, A., Kümmerli, R., and Rankin, D.J. (2014). Interaction
552 effects of cell diffusion, cell density and public goods properties on the evolution of
553 cooperation in digital microbes. J. Evol. Biol. *27*, 1869–1877.
554 43. López, D., and Kolter, R. (2010). Extracellular signals that define distinct and coexisting cell

555 fates in *Bacillus subtilis*. FEMS Microbiol. Rev. *34*, 134–49.
556 44. Winkelman, J.T., Bree, A.C., Bate, A.R., Eichenberger, P., Gourse, R.L., and Kearns, D.B. (2013).
557 RemA is a DNA-binding protein that activates biofilm matrix gene expression in *Bacillus*
558 *subtilis* . Mol. Microbiol. *88*, 984–997.
559 45. Elsholz, A.K.W., Wacker, S.A., and Losick, R. (2014). Self-regulation of exopolysaccharide
560 production in *Bacillus subtilis* by a tyrosine kinase. Genes Dev. *28*, 1710–1720.
561 46. Erskine, E., Morris, R., Schor, M., Earl, C., Gillespie, R.M.C., Bromley, K., Sukhodub, T., Clark, L.,
562 Fyfe, P., Serpell, L., *et al.* (2017). Formation of functional, non-amyloidogenic fibres by
563 recombinant *Bacillus subtilis* TasA. bioRxiv, 188995.
564 47. Allen, B., Gore, J., and Nowak, M.A. (2013). Spatial dilemmas of diffusible public goods. Elife
565 *2*, e01169.
566 48. Alteri, C.J., Himpsl, S.D., Pickens, S.R., Lindner, J.R., Zora, J.S., Miller, J.E., Arno, P.D., Straight,
567 S.W., and Mobley, H.L.T. (2013). Multicellular bacteria deploy the type VI secretion system to
568 preemptively strike neighboring cells. PLoS Pathog. *9*, e1003608.
569 49. Štefanič, P., Kraigher, B., Lyons, N.A., Kolter, R., and Mandić-Mulec, I. (2015). Kin
570 discrimination between sympatric *Bacillus subtilis* isolates. Proc. Natl. Acad. Sci. *112*, 14042–
571 14047.
572 50. Lyons, N.A., Kraigher, B., Štefanič, P., Mandić-Mulec, I., and Kolter, R. (2016). A combinatorial
573 kin discrimination system in *Bacillus subtilis*. Curr. Biol. *26*, 733–742.
574
575
576 **FIGURE LEGENDS**
577
578 Figure 1. **Costs and benefits of matrix components EPS and TasA. (A)** To estimate the metabolic costs
579 of EPS and TasA production the matrix-deficient strains Δ*eps* and Δ*tasA* were competed against the
580 WT and against each other under conditions where matrix components are produced but not required
581 (see Methods). Relative fitness (W) was calculated for Δ*eps* (when competed against WT), Δ*tasA*
582 (when competed against WT), and Δ*eps* (when competed against Δ*tasA*). Relative fitness W
583 significantly larger than 1 indicates an advantage of a given strain in a given pair-wise competition. For
584 Δ*eps* vs WT n=13, p<003; for Δ*tasA* vs WT n=13, p<008; for Δ*tasA* vs WT n=8, p<007 (**p<0.01, ***
585 p<0.001). **(B)** Productivity of the WT, Δ*eps*, Δ*tasA* and Δ*eps*+Δ*tasA* co-culture (50:50 ratio) measured
586 as CFU/ml. Data points represent mean and error bars represent standard error obtained from
587 biological triplicates. **(C)** Brightfield images of pellicle morphology developed by the WT, matrix-
588 deficient mutants in monocultures and by the Δ*eps*+Δ*tasA* co-culture (50:50 ratio). The cartoons below

589 represent public goods produced by each culture. **(D)** To confirm that EPS and TasA can be shared and
590 thereby serve as public goods, the matrix-deficient strains Δ*eps* and Δ*tasA* were allowed to form
591 pellicles in presence of spent media (SM) obtained from the WT or from the complementary mutant
592 (n=4-6). Pellicle productivity [CFU/ml] reached in presence of those SMs was compared with the
593 productivity of the control (a strain exposed to its own SM): for Δ*eps* + SM of WT $p<5x10^{-7}$; Δ*eps* + SM
594 of Δ*tasA* p<0.008; Δ*tasA* + SM of WT p<; Δ*tasA* + SM of Δ*eps* SM p<0.001 (**p<0.01). Boxes represent
595 Q1–Q3 (quartiles), lines represent the median, and bars span from max to min. To better distinguish
596 between the matrix-deficient mutants, data for Δ*eps* and Δ*tasA* are presented in pink and blue,
597 respectively.
598
599 Figure 2. **Native phenotypic heterogeneity in the expression of matrix components. (A)** Pellicles
600 formed by the double-labelled strain carrying the P_{eps}-*gfp* P_{tapA}-*mKate* reporters and the strain carrying
601 the P_{tapA}-*gfp* P_{tapA}-*mKate* reporters (control) were visualized using a confocal microscope to compare
602 the distribution of fluorescence signal from different fluorescence reporters (GFP, mKate). **(B)**
603 Volumes in GFP and mKate fluorescence channels (obtained by manual thresholding) were merged,
604 dissected into cubes and the average intensities in the GFP and mKate channels for all cubes were
605 plotted (see Methods). The maximum density is normalized to 1 and the contour lines correspond to
606 0.05 decrease in density. **(C)** The following strains: NCIB3610, NRS2242 (carrying P_{eps}-*gfp*), NRS3913
607 (carrying P_{tapA}-*mKate*), and NRS5832 (carrying P_{eps}-*gfp* and P_{tapA}-*mKate*); were allowed to form pellicles
608 and were then analyzed using flow cytometry. Bar chart (mean±SD) represents fraction of OFF cells,
609 cells expressing *eps-gfp*, *tapA-mKate*, and cells expressing both reporters (n=3).
610
611 Figure 3. **Productivity and fitness in pellicles with genetic division of labor. (A)** Productivities of
612 Δ*eps*+Δ*tasA* biofilms [CFU/ml] measured for different mixing ratios and compared to average
613 productivity reached by the WT (black horizontal line with grey shaded 95 % confidence interval). The
614 dashed line and green shaded 95% CI represent a cubic fit to the fitness data ($F_{3, 68} = 54.9$, $R^2 = 0.695$,
615 $p < 0.0001$). **(B)** The relative fitness of Δ*eps* in competition with Δ*tasA* followed a negative-frequency
616 dependent trajectory, best described by a cubic fit (dashed line with 95 % CI: $F_{3,46} = 94.7$, $R^2 = 0.852$, p
617 < 0.0001).
618
619 Figure 4. **Genetic division of labor on plant roots. (A)** *Arabidopsis thaliana* roots were colonized by
620 the WT, Δ*eps*+Δ*tasA* mix and the mutants in monocultures and biofilm productivities were measured
621 as CFU/mm of root (for WT and co-culture n=6; for Δ*eps* and Δ*tasA* n=11) (see Methods). The
622 productivity reached by the Δ*eps*+Δ*tasA* mixture was compared with productivity of the WT (p<0.04).

623 **(B)** *A. thaliana* roots were colonized by mixed cultures of WT_{GFP}+WT_{mKate}, Δeps_{GFP}+Δ$tasA_{mKate}$,
624 Δeps_{mKate}+Δ$tasA_{GFP}$ and the mutants in monocultures (Δeps_{GFP} and Δ$tasA_{GFP}$), and visualized using CLSM.
625 Scale bar represents 10µm. **(C)** Frequencies of each strain in the root-associated biofilm were
626 determined based on image analysis (see Methods). Bars represent average (n=3-5) and error bars
627 represent standard error.
628
629 Figure 5. **Individual-based simulations identify drivers of genetic division of labor.** We simulated
630 biofilm formation of the mutants Δ*eps* (producing TasA) and Δ*tasA* (producing EPS) when grown in co-
631 culture. Biofilms were initiated with eight cells, with Δ*eps* frequency varying between 0 and 1, in steps
632 of 0.125. Cells produced diffusible matrix components (either TasA or EPS) and grew according to their
633 fitness functions. After 10,000 time steps, we measured the absolute productivity of the biofilm (no.
634 of cells) and the relative fitness of the competing strains within biofilms. Fitness trajectories are shown
635 as the best fit from linear models across 50 simulations for each condition (± 95 % confidence interval).
636 **(A)** and **(B)** depict variation in biofilm productivity and relative fitness of mutants, respectively, as a
637 function of strain frequency and the matrix diffusion coefficient, under conditions where both matrix
638 components generate equal benefits. **(C)** and **(D)** show variation in biofilm productivity and relative
639 fitness of mutants, respectively, as a function of strain frequency and different relative benefits of the
640 two matrix components (diffusion coefficient d = 5). Dashed lines and grey shaded area in (**D)** depict
641 mean ± 95 % CI productivities of WT biofilms across a range of metabolic constraints (f) accruing in
642 the WT for simultaneously producing two public goods. **(E)** and **(F)** depict biofilm productivity and
643 relative fitness of a mutant growing together with the WT, respectively, as a function of strain
644 frequency and the matrix diffusion coefficient, under conditions where both matrix components
645 generate equal benefits.

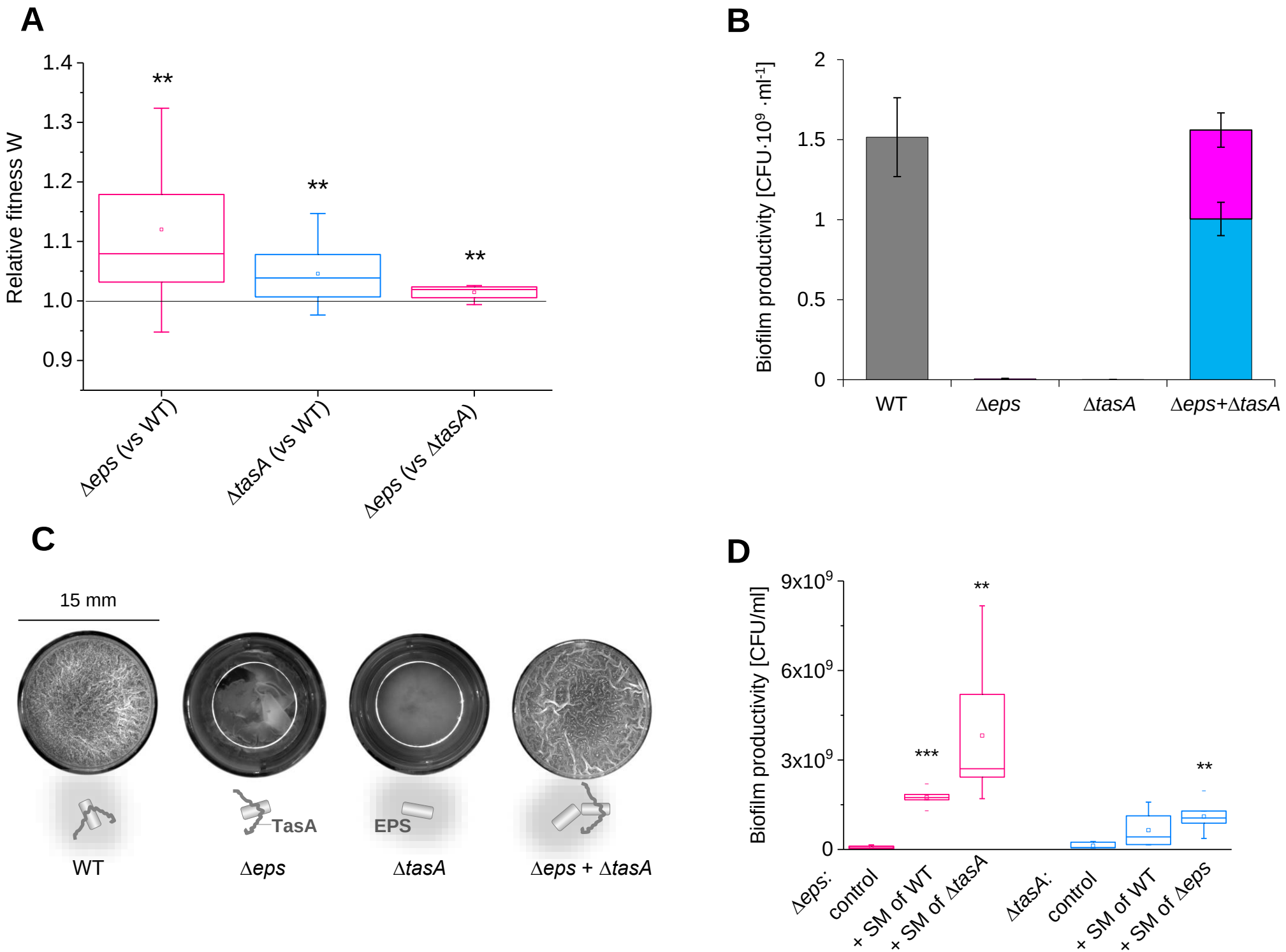
A
Relative fitness W
1.4
1.3
1.2
1.1
1.0
0.9
**
**
**
Δeps (vs WT)
ΔtasA (vs WT)
Δeps (vs ΔtasA)
B
Biofilm productivity [CFU·10⁹ ·ml⁻¹]
2
1.5
1
0.5
0
WT
Δeps
ΔtasA
Δeps+ΔtasA
C
15 mm
TasA
EPS
WT
Δeps
ΔtasA
Δeps + ΔtasA
D
Biofilm productivity [CFU/ml]
9x10⁹
6x10⁹
3x10⁹
0
***
**
**
Δeps:
control
+ SM of WT
+ SM of ΔtasA
ΔtasA:
control
+ SM of WT
+ SM of Δeps

A

B

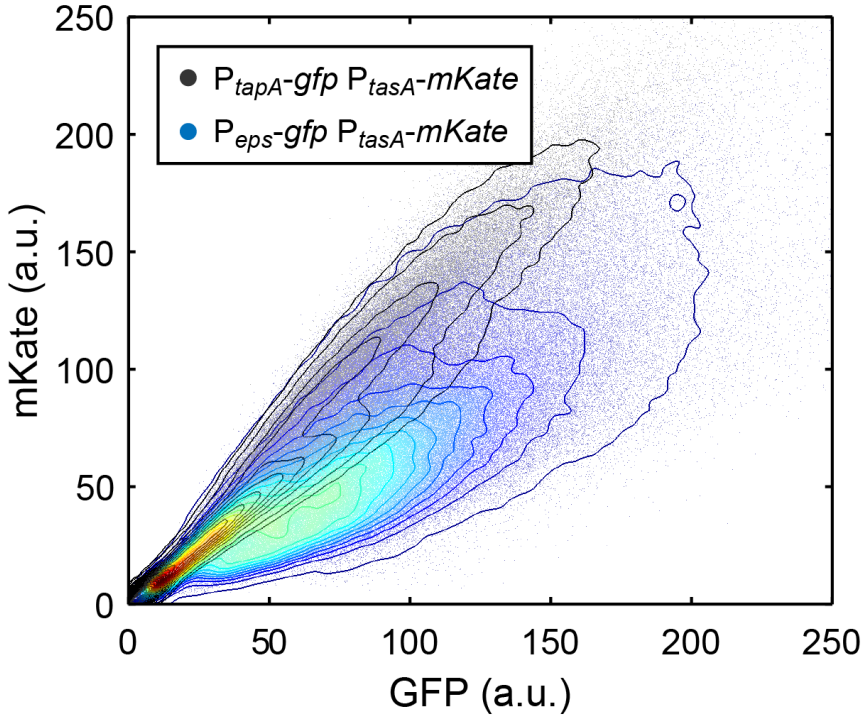
P_{tapA}-*gfp* P_{tasA}-*mKate*
P_{eps}-*gfp* P_{tasA}-*mKate*
mKate (a.u.)
GFP (a.u.)
0
50
100
150
200
250

C

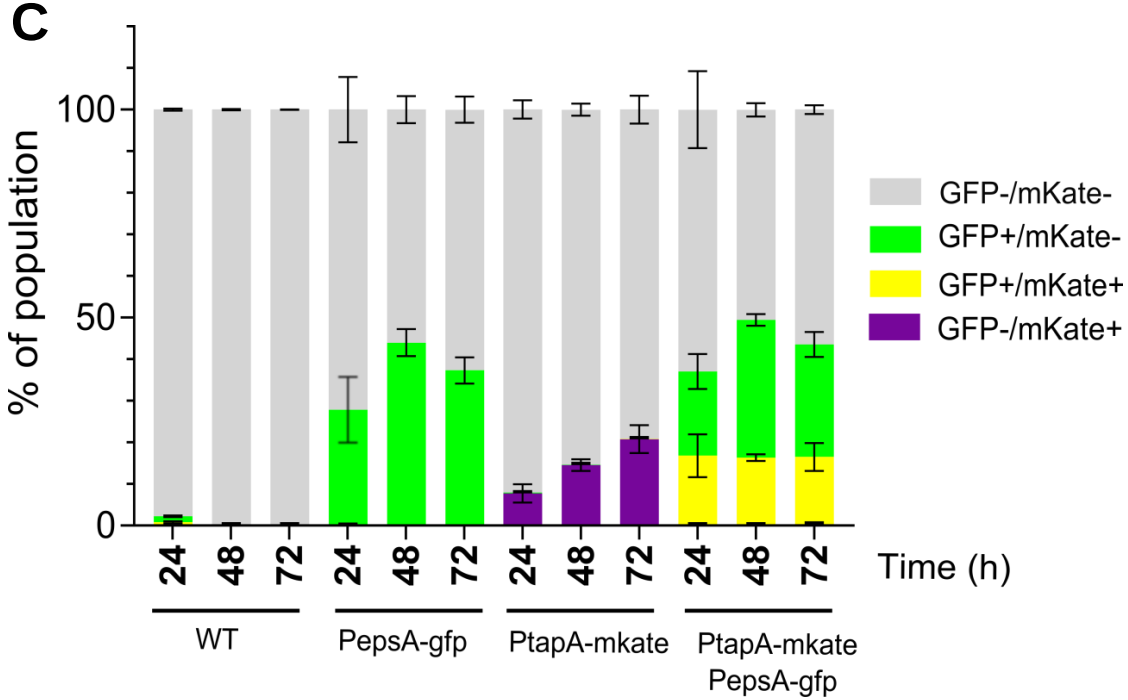
% of population
0
50
100
GFP-/mKate-
GFP+/mKate-
GFP+/mKate+
GFP-/mKate+
24
48
72
Time (h)
WT
PepsA-gfp
PtapA-mkate
PtapA-mkate
PepsA-gfp

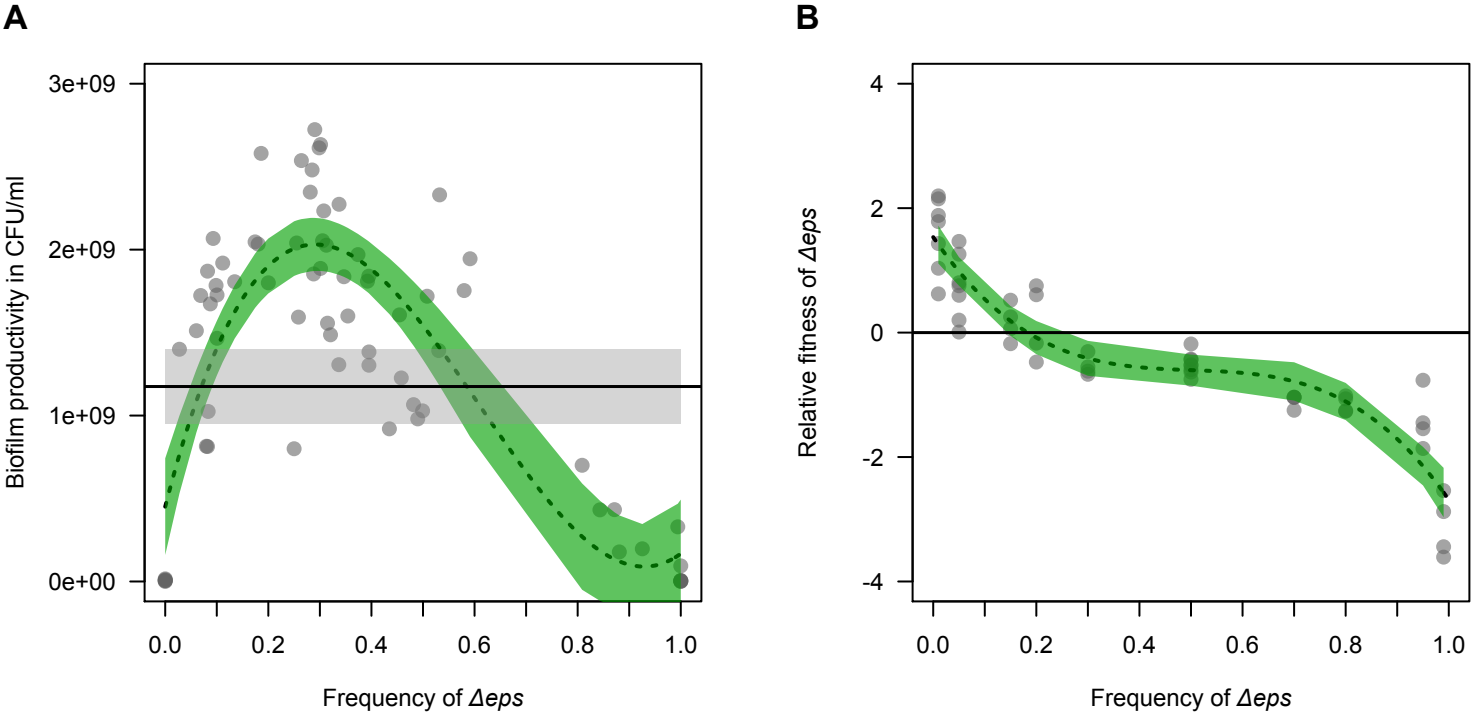
A
3e+09
2e+09
1e+09
0e+00
Biofilm productivity in CFU/ml
0.0
0.2
0.4
0.6
0.8
1.0
Frequency of Δeps
B
4
2
0
-2
-4
Relative fitness of Δeps
0.0
0.2
0.4
0.6
0.8
1.0
Frequency of Δeps

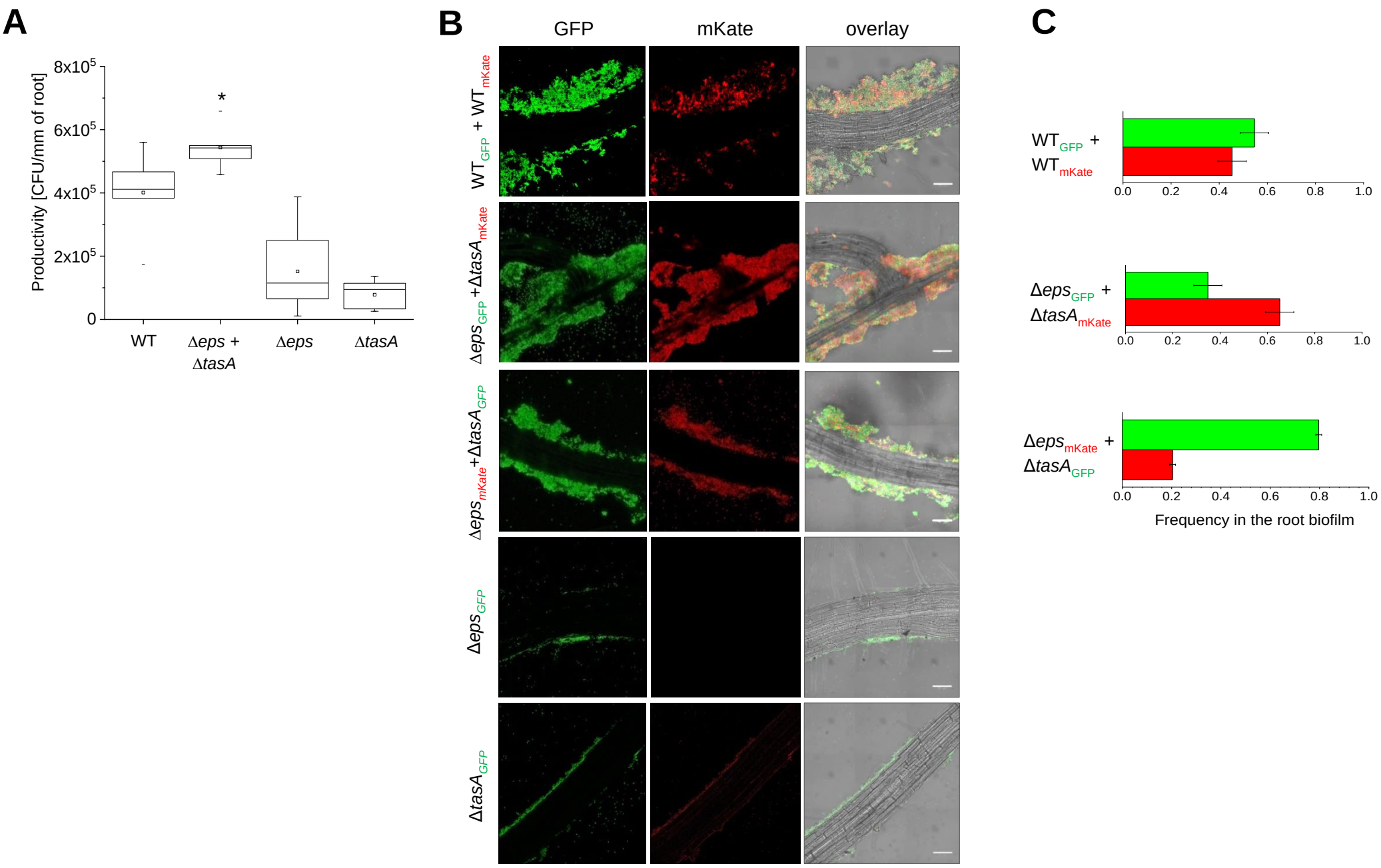
A
Productivity [CFU/mm of root]
8x10^5
6x10^5
4x10^5
2x10^5
0
*
WT
Δeps + ΔtasA
Δeps
ΔtasA
B
GFP
mKate
overlay
WT_GFP + WT_mKate
Δeps_GFP +ΔtasA_mKate
Δeps_mKate +ΔtasA_GFP
Δeps_GFP
ΔtasA_GFP
C
WT_GFP + WT_mKate
Δeps_GFP + ΔtasA_mKate
Δeps_mKate + ΔtasA_GFP
0.0
0.2
0.4
0.6
0.8
1.0
Frequency in the root biofilm

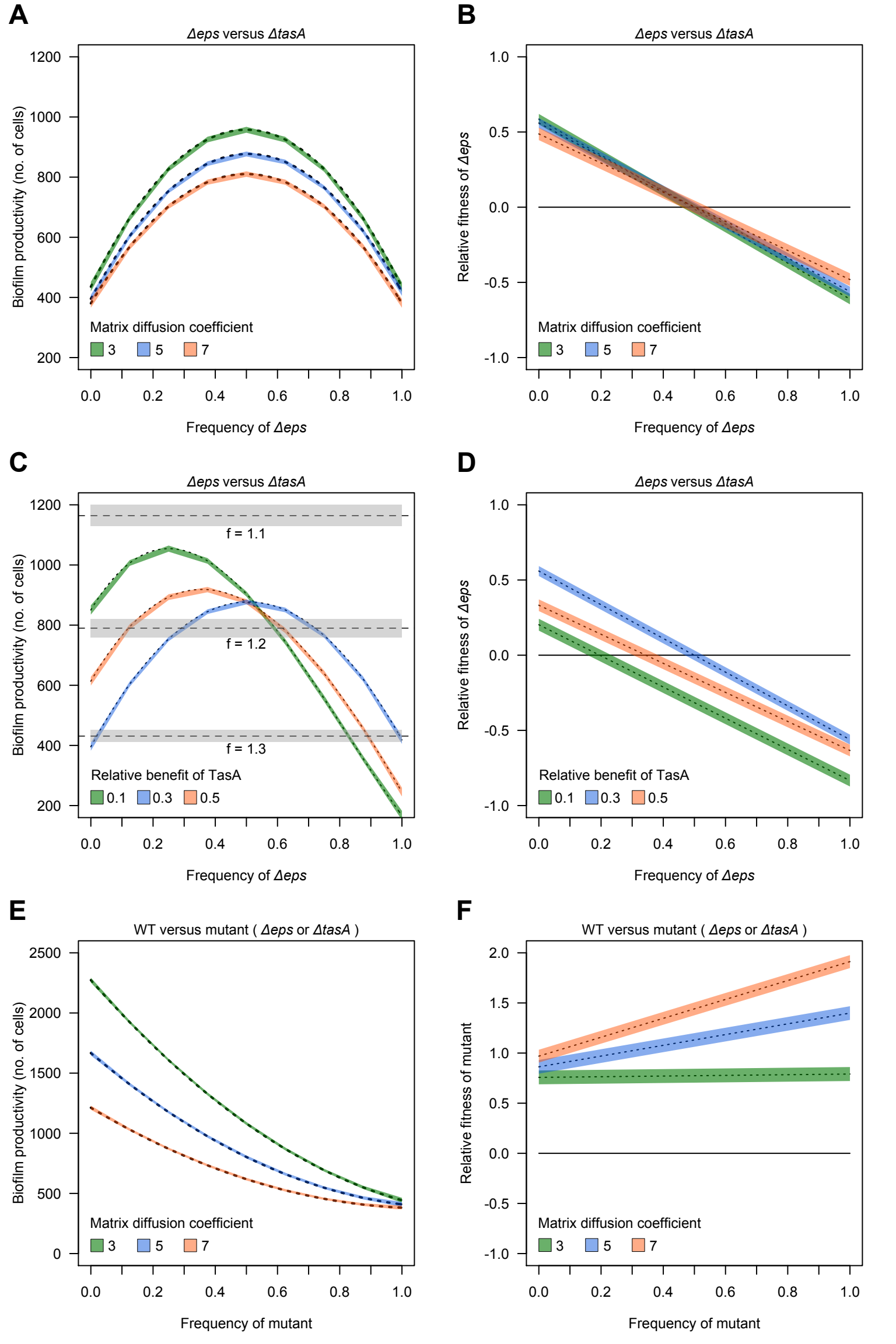
A
Δeps versus ΔtasA
Biofilm productivity (no. of cells)
Frequency of Δeps
Matrix diffusion coefficient
3
5
7
B
Δeps versus ΔtasA
Relative fitness of Δeps
Frequency of Δeps
Matrix diffusion coefficient
3
5
7
C
Δeps versus ΔtasA
f = 1.1
f = 1.2
f = 1.3
Biofilm productivity (no. of cells)
Frequency of Δeps
Relative benefit of TasA
0.1
0.3
0.5
D
Δeps versus ΔtasA
Relative fitness of Δeps
Frequency of Δeps
Relative benefit of TasA
0.1
0.3
0.5
E
WT versus mutant (Δeps or ΔtasA)
Biofilm productivity (no. of cells)
Frequency of mutant
Matrix diffusion coefficient
3
5
7
F
WT versus mutant (Δeps or ΔtasA)
Relative fitness of mutant
Frequency of mutant
Matrix diffusion coefficient
3
5
7

STAR*METHODS

CONTACT FOR REAGENT AND RESOURCE SHARING

Further information and requests for resources and reagents should be directed to and will be fulfilled by the Lead Contact, Ákos T. Kovács (atkovacs@dtu.dk).

EXPERIMENTAL MODEL AND SUBJECT DETAILS

All bacterial strains used in this study derived from *Bacillus subtilis* NCBI 3610 *comI*^{Q12I} strain (Konkol et al., 2013). Strains were maintained in LB medium (Lysogeny broth (Lennox); Carl Roth, Germany), while MSgg medium was used for pellicle formation assay [1].

METHOD DETAILS

Strain construction. All strains that were used in this study or that were used solely as gDNA donors are listed in Table S1. To obtain TB601 and TB863, the NCBI 3610 *comI*^{Q12I} was transformed with gDNA isolated from DL1032 selecting for Tet-resistant colonies or Km-resistant colonies, respectively.
TB524.1 and TB525.2 were obtained by transforming TB601 with gDNA isolated from TB500.1 and TB501.1, respectively. TB538.1 and TB539.1 were obtained by transforming TB602 with gDNA isolated from TB500.1 and TB501.1, respectively. To obtain TB864 and TB865, NCBI 3610 *comI*^{Q12I} was first transformed with gDNA from 168hymKate and then with gDNA isolated from NRS2242 and NRS3913, respectively. To obtain Anc Kate P_{eps}-GFP, strain TB602 was first transformed with gDNA from 168hymKate and then with gDNA from NRS2242. To obtain Anc Kate P_{tapA}-GFP, strain TB 601 was first transformed with gDNA from 168hymKate and then with gDNA from NRS2394. In order to construct pTB848 and pTB849, the *eps* and *tapA* promoters were amplified using oTB172-oTB173 and oTB174-oTB175 primers pairs, respectively (see Table S2), the PCR products were digested with *Eco*RI and *Nhe*I, and cloned into the corresponding sites of vector pmKATErrnB. To obtain strains TB961 and TB962, first NCBI 3610 *comI*^{Q12I} was transformed with gDNA from NRS2242, and the obtained strain (TB373) was transformed with plasmids pTB848 and pTB849, respectively. TB960 was constructed by transforming NCBI 3610 *comI*^{Q12I} with gDNA from NRS3913 and the obtained strain (TB363) was subsequently transformed with pTB849 plasmid. To construct plasmid pTB498 harbouring a constitutively expressed mKATE2 gene, the $P_{hyperspank}$-mKATE2 fragment was PCR amplified with primers oTH1 and oTH2 from plasmid phy-mKATE2 [2], digested with *Xba*I and *Eco*RI, ligated into

plasmid pWK-Sp as described in [3]. Resulting plasmids were verified by sequencing and transformed into *B. subtilis* NCBI 3610 *comI*^{Q12I}, resulting in TB539.

Plasmid pNW725 was used to construct strain NRS3913. This was generated through amplification of the *mKate2* coding region from plasmid pTMN387 using primers NSW1026 and NSW1027 (see Table S2) and ligation into plasmid pNW600 using *HinD*III and *Bam*HI. Plasmid pNW600 carries the P*tapA* promoter region (Murray et al., 2009), and therefore plasmid pNW725 has the *mKate2* coding region under the control of the *tapA* promoter region. Plasmid pNW725 was integrated into the chromosome of *B. subtilis* NCIB3610 at the *amyE* locus. Strain NRS5832 was generated by phage transduction of the P*epsA-gfp* reporter fusion from strain NRS2242 into NRS3913 as the recipient. Phage transduction was performed using SSP1 phage as previously described (Verhamme et al., 2007).

Pellicle formation and productivity assays. To obtain pellicle biofilms, bacteria were routinely growth in static liquid MSgg medium at 30°C for 48 hours, using 1% inoculum from overnight cultures. Productivities where accessed by examining colony forming units (CFUs) in mature pellicles. Prior each CFU assays, pellicles were sonicated according to a protocol optimized in our laboratory that allows proper disruption of biofilms without affecting cell viability [4,5]. To access relative frequencies of Δ*eps* and Δ*tasA* strains, the cocultures were plated on selective antibiotics tetracycline (10µg/ml) and spectinomycin (100µg/ml), respectively.

Fitness assays. Since the expression of *epsA-O* and *tapA-sipW-tasA* operons strongly depend on cultivation conditions and media composition [3,6–9], we performed the competition experiment for the fitness costs of EPS and TasA production under the same conditions that were later used for the assays that involved pellicles. Strains of interest were premixed at 1:1 ratios based on their OD_{600} values and the mixture was inoculated into MSgg medium at 1%. Cultures were grown under static conditions at 30°C. CFU assays (using selective antibiotics for the Δ*eps* and Δ*tasA* strains) were performed immediately after inoculation and after 16 hours of growth. The growth curves obtained at the initial stage of pellicle formation were performed under standard pellicle growth conditions in 96-well plates. The optical densities and GFP-fluorescence were monitored using an infinite F200PRO plate reader (TECAN Group Ltd, Männedorf, Switzerland).

Spent media complementation assay. The supernatants were obtained from the WT, Δ*eps* and Δ*tasA* strains grown under static conditions in MSgg medium at 30°C for 48 hours. Cells were pelleted by centrifugation (5min, 8000 r.p.m.), the supernatants were sterilized using Millipore filters (0.2µm pore size), and mixed in 1:1 ratio with 2 times´ concentrated MSgg medium. Surface colonization of the

Δ*eps* and Δ*tasA* in presence of conditioned media from the WT or complementary mutant strains were compared with the negative controls where the mutants grew in presence of their own conditioned media.

Microscopy/confocal laser scanning microscopy (CLSM). Bright field images of whole pellicles and colonies were obtained with an Axio Zoom V16 stereomicroscope (Carl Zeiss, Jena, Germany) equipped with a Zeiss CL 9000 LED light source and an AxioCam MRm monochrome camera (Carl Zeiss). For time-lapse experiment, cultures were grown in 24-well plates (1.5 cm diameter per well), incubated in INUL-MS2-F1 incubator (Tokai Hit, Shizuoka, Japan) at 30 °C and images were recorded every 15 min. The detailed description of the fluorescence time lapse microscope has been previously published [10]. The pellicles were also analyzed using a confocal laser scanning microscope (LSM 780 equipped with an argon laser, Carl Zeiss) and Plan-Apochromat/1.4 Oil DIC M27 63× objective. Fluorescent reporter excitation was performed with the argon laser at 488 nm and the emitted fluorescence was recorded at 484–536 nm and 567–654 nm for GFP and mKate, respectively. To generate pellicle images, Z-stack series with 1 µm steps were acquired. Zen 2012 Software (Carl Zeiss) was used for both stereomicroscopy and CLSM image visualization.

Sample fixing and flow cytometry. Pellicles were harvested at 24, 48, and 72 h into sterile 2 ml screw cap tubes, followed by centrifugation at 17000´g for 10 min. GTA buffer (50 mM glucose, 10 mM EDTA pH 8.0, and 20 mM Tris-HCl pH 8.0) was added into 24-well plates to harvest the cells remained in wells and pooled with cell pellet from previous step. Pooled cell pellets were then pumped through 23G needles 6 times to disperse pellicles. Dispersed samples were pelleted down and fixed by incubation with 4% paraformaldehyde for 7 min at room temperature. Fixed samples were washed with GTA, and subjected to mild sonication prior flow cytometry. Flow cytometry (LSRFortessa™, BD biosciences) were operated by FACS facility in School of Life Sciences, University of Dundee. For initial experiments comparing the expression of matrix genes in the WT and the biofilm mutants flow cytometry (BD Facscanto II, BD biosciences) was performed at Disease Systems Immunology Group, DTU Bioengineering.

Root colonization assay/root biofilms productivity. Colonization of *Arabidopsis thaliana* roots was performed according to modified protocol from [7]. Arabidopsis ecotype Col-0 seeds were surface sterilized using 2% (v/v) sodium hypochlorite solution as follows: seeds were incubated in 2% (v/v) sodium hypochlorite with mixing on an orbital shaker for 20 min and then washed five times with sterile distilled water. The seeds were placed on pre-dried MS agar plates (Murashige and Skoog basal

salts mixture; Sigma) (2.2 g l^{-1}) in an arrangement approximately 20 seeds per plate at a minimum distance of 1 cm. Seeds were germinated and grown on agar plates containing MS medium. After 3 days of incubation at 4°C, plates were placed at an angle of 65° in a plant chamber (21°C, 16h light per day). After 6 days, homogenous seedlings ranging 0.8-1.2cm in length were selected for root colonization assay. Seedlings were transferred into 48-well plates containing 270µl of MSNg medium [7]per well. Next the medium was supplemented with 30µl of exponentially growing bacterial culture diluted to OD_{650} = 0.2. The sealed plates were incubated at rotary shaker at 28°C for 18h at 90 r.p.m. After the incubation, plants were washed 3 times with MSNg to remove non-attaching cells and then transferred to a glass slide for imaging using CLSM. To access root biofilm productivities, the roots were transferred into Eppendorf tubes, subjected to standard sonication protocol and the CFU assays were performed for obtained cell suspensions. To extract CFU/mm of root, the obtain CFU values were divided by total length of a corresponding root.

Images of plant roots. For biofilm roots visualization, the GFP and mKate images were converted into 3D projections, contrast was enhanced using normalized function and green and red lookup tables were applied for GFP and mKate channels, respectively. Overlay images were obtained in ZEN software and further processed using ImageJ as follows: Brightness and contrast were adjusted, the root and biofilm area was manually selected and the background was lightened and smoothed using 'adjust brightness' and 'smooth' functions, respectively.

Modelling. We performed individual-based simulations, using the platform developed by Dobay et al. (2014). Microbial simulations occur on a two-dimensional toroidal surface with connected edges (i.e. there are no boundaries). The surface of the torus is 10,000 μm^2 (100 x 100 µm). Bacteria are modeled as discs with an initial radius of 0.5 µm. Bacteria can consume resources, grow at a basic growth rate (μ = 1) and divide when reaching the threshold radius of 1 µm. In our simulations, we assumed that resources are not limited. Bacteria further produce beneficial public goods at a cost c per molecule and at constant rate of 1 molecule/s. Public goods diffuse randomly according to the diffusion coefficient d (μm^2/s) and following a Gaussian random walk. Public goods can decay with a certain probability p, with p increasing exponentially with time following the exponential function $p = 1 - e^{-w\Delta t/\partial}$, where Δt is the age of the molecule, w the stiffness of the decay and ∂ the durability of the molecule. A public good can generate a benefit b to the cell that takes it up, which occurs when the cell and the public good physically overlap on the landscape. Bacteria can randomly disperse, too, defined by the diffusion coefficient D (μm^2/s). Because we aimed to model bacterial performance in biofilms, where cell dispersal is relatively low, we set D = 0.01 μm^2/s. Important to note is that neither

bacteria nor public goods are bound to a grid, but move on a continuous landscape (following an off-lattice model with double-precision numbers). This mimics natural bacterial behavior as close as possible. One practical complication of this approach is that cells overlap with each other following diffusion. To cope with this issue, we applied an overlap correction after each time step following the procedure described in [11].

Using this setup, we simulated the performance of a wildtype (WT) strain, producing two public goods representing EPS and TasA, and two strains (PG1 and PG2) producing only one of the two public goods. We arbitrarily considered PG1 = TasA producer and PG2 = EPS producer. The growth of the three strains is defined by the following recursive functions:

$$G_{WT}(t+1) = [\mu - f(c_1 + c_2) + b_1 \sum pg1 + b_2 \sum pg2 + b_3\left(\sum pg1 + R_{pg1}\right)\left(\sum pg2 + R_{pg2}\right)]G_{WT}(t) \quad (1)$$

$$G_{PG1}(t+1) = [\mu - c_1 + b_1 \sum pg1 + b_2 \sum pg2 + b_3\left(\sum pg1 + R_{pg1}\right)\left(\sum pg2 + R_{pg2}\right)]G_{PG1}(t) \quad (2)$$

$$G_{PG2}(t+1) = [\mu - c_2 + b_1 \sum pg1 + b_2 \sum pg2 + b_3\left(\sum pg1 + R_{pg1}\right)\left(\sum pg2 + R_{pg2}\right)]G_{PG2}(t) \quad (3)$$

where G is the radius increase per time step t, μ is the basic growth rate, c_1 and c_2 are the costs of producing the respective public goods, and f is the metabolic constraint factor, whereby $f > 1$ if the simultaneous production of both public goods is costlier than producing either of the public goods alone. Furthermore, while b_1 and b_2 are the benefits accruing when a respective public good is taken up multiplied by the total number of public goods consumed ($\Sigma pg1$ and $\Sigma pg2$) per time step, b_3 is the synergistic benefit accruing for all the complementary public goods taken up within a certain period of time (R_{pg1} and R_{pg2}, respectively). We arbitrarily chose five time steps for R_{pg1} and R_{pg2}.

For all simulations, we seeded our in-silico landscape with eight cells placed in the center of the landscape to mimic the early phase of pellicle formation. Cells then started to produce public goods, grew and divided defined by their growth function. We let bacteria grow for 10,000 time steps in 50 independent replicates for each parameter combination. We examined three growth treatments, which included the WT strain in monoculture, the two complementary strains PG1 and PG2 in

monocultures, and the two complementary strains PG1 and PG2 in mixed cultures. In the mixed cultures, we varied the starting frequency of the two strains from 1:7 (PG1 to PG2) to 7:1. For all simulations, we extracted the absolute productivity of the biofilm and the relative fitness of the competing strains within biofilms. To assess the role of public good diffusion on biofilm productivity and relative strain fitness, we varied public good diffusion from 3 to 7 $\mu m^2/s$ in steps of 0.5 $\mu m^2/s$. To take into account that the public goods TasA and EPS might generate different benefits we varied the b_1/b_2 ratio from 1/9 to 1/1. Finally, we examined the effect of metabolic constraints on WT fitness by varying f from 1 to 1.3. All parameters together with the specific values used are given in the Supplementary Table S3.

QUANTIFICATION AND STATISTICAL ANALYSIS

Relative fitness. Relative fitness W_A for strain A in competition with strain B was calculated as follows:

$$W_A = [\ln(CFU_{A_16h}/CFU_{A_start})]/[\ln(CFU_{B_16h}/CFU_{B_start})]$$

All replicates where one strain occurred to strongly dominate in the initial inoculum (exceeding initial 0.8 frequency) were removed from the dataset.

Strain frequencies on plant roots. Ratios of the Δ*eps*^{GFP} and ΔtasA^{mKate} (and control with swapped fluorescent reporters) in root biofilms were estimated from the ratios of white pixel volumes measured on corresponding fluorescent images. Images were analyzed using ImageJ software. First, the root and biofilm area it was manually selected on the white-light image. For each channel, the stacks were converted into binary images and threshold was set up to > 0 value. Next, the root+biofilm selection was activated on the processed stacks and total pixel volumes for each channel were extracted using 'stacks statistics' function.

Density correlation. The corresponding image stacks were dissected into cubes of 10 px side length. For each channel, the biovolume per cube was obtained. For all cubes containing biovolume in either of the two fluorescence channels (designated ch1 and ch2) the total biovolume in ch1 and ch2 within a sphere of a given radius (1 - 5 µm) was summed up, multiplied and normalized by the total volume of the sphere.

The resulting value ranges from 0 (no correlation, no biomass in one of the channels) over 0.25 (50% of biomass in ch1, 50% of biomass in ch2) to 1 (cube is completely filled in both channels = 100% overlap).

Statistical analysis. For relative fitness assay, statistical differences from W=1 were identified using one-sample Student's t-test. In case of productivity measurements statistical differences between two experimental groups were identified using two-tailed Student's *t*-tests assuming equal variance. Variances in the two main types of datasets (relative fitness, productivity) were similar across different samples. No statistical methods were used to predetermine sample size and the experiments were not randomized. All relevant data are available from the authors.

KEY RESOURCES TABLE

Reagent or Resource	Source	Identifier
Chemicals		
Lysogeny broth (LB), Lennox	Carl Roth GmbH	X964.1
Agar-Agar	Carl Roth GmbH	5210.3
Potassium Hydrogen Phosphate	Carl Roth GmbH	P749.1
Potassium Dihydrogen Phosphate	Carl Roth GmbH	3904.2
L-Glutamic acid Monopotassium salt monohydrate	Alfa Aesar	17232
Magnesium chloride hexahydrate	Carl Roth GmbH	2189.1
Potassium chloride	Carl Roth GmbH	6781.3
Calcium chloride	Carl Roth GmbH	5239.2
Manganese(II) chloride	Carl Roth GmbH	T881.3
Iron(III) chloride	Carl Roth GmbH	P742.1
Zinc chloride	Carl Roth GmbH	T887.1
Ammonium chloride	Carl Roth GmbH	K298.2
Thiamin	Carl Roth GmbH	T911.1
MOPS	Carl Roth GmbH	6979.4
Glycerol	Carl Roth GmbH	7533.1
Murashige and Skoog medium (MS)	Sigma Aldrich	M5519
Sodium hypochlorite	Carl Roth GmbH	9062.3
Tetracycline hydrochloride	Carl Roth GmbH	0237.1
Spectinomycin dihydrochloride	Alfa Aesar	J61820
Glucose	Fisher Scientific	G/0500/61
EDTA	VWR	20302.260
Tris	VWR	103157P
HCl	VWR	20252.335
Experimental Models: Organisms/Strains		
Bacillus subtilis NCBI 3610 *comI*^{Q12I}	[12]	DK1042
Bacillus subtilis NCBI 3610 *comI*^{Q12I} *derivatives (listed in Table S2).*	This study	N/A
Arabidopsis thaliana Col-0	Greenhouse of Max Plank Institute for Chemical Ecology, Jena	N/A
Recombinant DNA		

pmKATErrnB	[2]	Genbank Accession number: KF245454
pTB848	This study	N/A
pTB849	This study	N/A
pTB498	This study	N/A
pNW725	This study	N/A
Sequence-Based Reagents		
Primers used in this study are listed in Table S3.	This study	N/A
Software and Algorithms		
ImageJ	[13]	https://imagej.nih.gov/ij/
OriginPro 2015G	OriginLab, Northampton, MA	http://www.originlab.com/

Supplementary Tables

Table S1. Bacterial strains used during experiments or as a source of genomic DNA

Strain name	Genotype	Reference
DL1032	*eps*::*tet, tasA*::*Km, amyE*::P_{srfAA}-*lacZ (ery)*	[14]
NCIB3610	*Prototroph*	NSW laboratory
TB601	3610 *comI*^{Q12l} *eps*::*tet*	This work
TB602	3610 *comI*^{Q12l} *tasA*::*spec*	[3]
TB863	3610 *comI*^{Q12l} *tasA*::*kan*	This work
TB500	3610 *comI*^{Q12l} *amyE*::$P_{hyperspank}$-GFP (Spec^R)	[3]
TB501	3610 *comI*^{Q12l} *amyE*::$P_{hyperspank}$-mKate (Spec^R)	This work
TB524	3610 *comI*^{Q12l} *eps*::*tet amyE*::$P_{hyperspank}$-GFP (Spec^R)	This work
TB525	3610 *comI*^{Q12l} *eps*::*tet amyE*::$P_{hyperspank}$-mKate (Spec^R)	This work
TB538	3610 *comI*^{Q12l} *tasA*::*kan amyE*::$P_{hyperspank}$-GFP (Spec^R)	This work
TB539	3610 *comI*^{Q12l} *tasA*::*kan amyE*::$P_{hyperspank}$-mKate (Spec^R)	This work
168hymKate	168 *amyE*::$P_{hyperspank}$-mKATE2 (Cm^R)	[2]
TB864	3610 *comI*^{Q12l} *amyE*::$P_{hyperspank}$-mKate (Cm^R) *sacI*::P_{eps}-*gfp* (Km^R)	This work
TB865	3610 *comI*^{Q12l} *amyE*::$P_{hyperspank}$-mKate (Cm^R) *sacI*::P_{tapA}-*gfp* (Km^R)	This work
Anc Kate P_{eps}-GFP	3610 *comI*^{Q12l} *tasA*::*spec* amyE::$P_{hyperspank}$-mKate (Cm^R) *sacI*::P_{eps}-*gfp* (Km^R)	This work
Anc Kate P_{tapA}-GFP	3610 *comI*^{Q12l} *eps*::*tet* amyE::$P_{hyperspank}$-mKate (Cm^R) *sacI*::P_{tapA}-*gfp* (Km^R)	This work
TB960	3610 *comI*^{Q12l} *amyE*::P_{tapA}-*mKate* (Cm^R) *sacI*::P_{eps}-*gfp* (Km^R)	This work
TB961	3610 *comI*^{Q12l} *amyE*::P_{eps}-*mKate* (Cm^R) *sacI*::P_{tapA}-*gfp* (Km^R)	This work
TB962	3610 *comI*^{Q12l} *amyE*::P_{tapA}-*mKate* (Cm^R) *sacI*::P_{tapA}-*gfp* (Km^R)	This work
NRS2394	3610 *sacA*::P_{tapA}-*gfp* (Km^R)	[15]
NRS3913	3610 *amyE*::P_{tapA}-*mKate2* (Cm^R)	This work
NRS2242	3610 *sacI*::P_{eps}-*gfp* (Km^R)	[15]
NRS5832	3610 *sacI*::P_{eps}-*gfp* (Km^R) *amyE*::P_{tapA}-*mKate2* (Cm^R)	This work

Table S2. Primers used in this study

Primer	Experimental purpose	Sequence
oTB172	Cloning *eps* promoter into pmKATErrnB	CACGAATTCCAACAGCCAGCTGATTAATAG
oTB173	Cloning *eps* promoter into pmKATErrnB	CTGAGCTAGCCATTTCCTCTCCTCCTTCCCGCGGCTGGCTTC
oTB174	Cloning *tapA* promoter into pmKATErrnB	CACGAATTCCCTTCCCTCAGAGTTAAATG

oTB175	Cloning *tapA* promoter into pmKATErrnB	CTGAGCTAGCCATTTCCTCTCCTCCTGTAAAACACTGTAAC
oTH1	Cloning $P_{hyperspank}$-mKate into pWK-Sp	GCATCTAGAGTTGCTCGCGGGTAAATGTG
oTH2	Cloning $P_{hyperspank}$-mKate into pWK-Sp	CGAGAATTCATCCAGAAGCCTTGCATATC
NSW1026	Amplification *mKate2* from plasmid pTMN387	GTACAAGCTTAAGGAGGAACTACTATGGATTCAATAGAAAAGGTAAG
NSW1027	Amplification *mKate2* from plasmid pTMN387	GTACGGATCCTTATCTGTGCCCCAGTTTGCT

Table S3. Parameters and specific values used in modeling

Parameter	**Description**	**Value(s)**
μ	basic growth rate	1
D	cell diffusion	0.01
d	public good diffusion	3 - 7 $\mu m^2/s$
ω	stiffness of decay function	0.1
δ	public good durability	500 s
c_1	cost of public good 1 (TasA)	0.0005 per molecule
c_2	cost of public good 2 (EPS)	0.0005 per molecule
f	metabolic constraint factor	1 - 1.3
b_1	benefit of public good 1 (TasA)	0.0001 - 0.0009
b_2	benefit of public good 2 (EPS)	0.0001 - 0.0009
b_3	synergistic benefit	0.0005

1. Branda, S.S., Gonzalez-Pastor, J.E., Ben-Yehuda, S., Losick, R., and Kolter, R. (2001). Fruiting body formation by Bacillus subtilis. Proc. Natl. Acad. Sci. U. S. A. *98*, 11621–11626.

2. van Gestel, J., Weissing, F.J., Kuipers, O.P., and Kovács, Á.T. (2014). Density of founder cells affects spatial pattern formation and cooperation in Bacillus subtilis biofilms. ISME J. *8*, 2069–79.

3. Mhatre, E., Sundaram, A., Hölscher, T., Mühlstädt, M., Bossert, J., and Kovács, Á.T. (2017). Presence of calcium lowers the expansion of *Bacillus subtilis* colony biofilms. Microorganisms *5*, 7.

4. Martin, M., Dragoš, A., Hölscher, T., Maróti, G., Bálint, B., Westermann, M., and Kovács, Á.T.

(2017). *De novo* evolved interference competition promotes the spread of biofilm defectors. Nat. Commun. *8*, 15127.

5. Dragoš, A., Lakshmanan, N., Martin, M., Horváth, B., Maróti, G., García, C.F., Lieleg, O., and Kovács, Á.T. (2017). Evolution of exploitative interactions during diversification in *Bacillus subtilis* biofilms. FEMS Microbiol. Ecol.

6. Rubinstein, S.M., Kolodkin-Gal, I., Mcloon, A., Chai, L., Kolter, R., Losick, R., and Weitz, D.A. (2012). Osmotic pressure can regulate matrix gene expression in *Bacillus subtilis* . Mol. Microbiol. *86*, 426–436.

7. Beauregard, P.B., Chai, Y., Vlamakis, H., Losick, R., and Kolter, R. (2013). *Bacillus subtilis* biofilm induction by plant polysaccharides. Proc. Natl. Acad. Sci. *110*, 1621–1630.

8. Shemesh, M., Kolter, R., and Losick, R. (2010). The biocide chlorine dioxide stimulates biofilm formation in *Bacillus subtilis* by activation of the histidine kinase KinC. J. Bacteriol. *192*, 6352–6.

9. Shemesh, M., and Chai, Y. (2013). A combination of glycerol and manganese promotes biofilm formation in Bacillus subtilis via histidine kinase KinD signaling. J. Bacteriol. *195*, 2747–2754.

10. Hölscher, T., Dragoš, A., Gallegos-Monterrosa, R., Martin, M., Mhatre, E., Richter, A., and Kovács, Á.T. (2016). Monitoring spatial segregation in surface colonizing microbial populations. J. Vis. Exp.

11. Dobay, A., Bagheri, H.C., Messina, A., Kümmerli, R., and Rankin, D.J. (2014). Interaction effects of cell diffusion, cell density and public goods properties on the evolution of cooperation in digital microbes. J. Evol. Biol. *27*, 1869–1877.

12. Konkol, M.A., Blair, K.M., and Kearns, D.B. (2013). Plasmid-encoded ComI inhibits competence in the ancestral 3610 strain of *Bacillus subtilis*. J. Bacteriol. *195*, 4085–4093.

13. Schindelin, J., Arganda-Carreras, I., Frise, E., Kaynig, V., Longair, M., Pietzsch, T., Preibisch, S., Rueden, C., Saalfeld, S., Schmid, B., *et al.* (2012). Fiji: an open-source platform for biological-image analysis. Nat. Methods *9*, 676–682.

14. López, D., Vlamakis, H., Losick, R., and Kolter, R. (2009). Paracrine signaling in a bacterium. Genes Dev. *23*, 1631–8.

15. Murray, E.J., Strauch, M.A., and Stanley-Wall, N.R. (2009). X Is involved in controlling *Bacillus subtilis* biofilm architecture through the AbrB homologue Abh. J. Bacteriol. *191*, 6822–6832.